Journal of Engineering Mathematics **44:** 369–394, 2002.

Similarity solutions for slender dry patches with thermocapillarity

D. HOLLAND, S. K. WILSON[1] and B. R. DUFFY[2]
Department of Mathematics, University of Strathclyde, Livingstone Tower, 26 Richmond Street, Glasgow G1 1XH, UK

Received 19 February 2002; accepted in revised form 12 August 2002

Abstract. The lubrication approximation is used to investigate slender dry patches in an infinitely wide film of viscous fluid flowing steadily on an inclined plane that is either heated or cooled relative to the surrounding atmosphere. Four non-isothermal situations in which thermocapillary effects play a significant role are considered.

Similarity solutions describing a thermocapillary-driven flow with a dry patch that is widening or narrowing due to either gravitational or surface-tension effects on a non-uniformly heated or cooled substrate are obtained, and examples of these solutions, when the substrate temperature gradient depends on the longitudinal coordinate according to a general power law, are presented. When gravitational effects are strong, the solution contains a free parameter, and for each value of this parameter there is a unique solution representing both a narrowing pendent dry patch and a widening sessile dry patch, whose transverse profile has a monotonically increasing shape. When surface-tension effects are strong, the solution also contains a free parameter, and for each value of this parameter there is both a unique solution representing a narrowing dry patch, whose transverse profile has a monotonically increasing shape, and a one-parameter family of solutions representing a widening dry patch, whose transverse profile has a capillary ridge near the contact line and decays in an oscillatory manner far from it.

Similarity solutions are also obtained for both a gravity-driven and a constant-surface-shear-stress-driven flow with a dry patch that is widening or narrowing due to thermocapillarity on a uniformly heated or cooled substrate. The solutions in both cases contain a free parameter, and for each value of this parameter there is a unique solution representing both a narrowing dry patch on a heated substrate and a widening dry patch on a cooled substrate, whose transverse profile has a monotonically increasing shape.

Key words: contact line, dry patch, gravity, lubrication approximation, thermocapillarity

1. Introduction

The formation, shape and stability of dry patches in thin fluid films flowing on solid substrates is a much studied problem with numerous practical applications, including heat exchangers, nuclear reactors, liquid-cooled turbine blades and falling-film evaporators. In this paper we shall consider dry patches in an infinitely wide fluid film driven by gravity, thermocapillarity or a constant surface shear stress flowing steadily on a heated or cooled inclined plane when thermocapillary effects play a significant role.

The pioneering work on a dry patch in an isothermal infinitely wide film of viscous fluid draining steadily under gravity down an inclined plane was performed by Hartley and Murgatroyd [1], who proposed a condition for the critical maximum volume flux for a dry patch to persist based on a balance between surface tension and inertia forces at the stagnation point at its apex. Experiments (see, for example, the photographs of Ponter *et al.* [2] and Podgorski *et al.* [3]) reveal the presence of a distinctive 'capillary ridge' near the contact line which is

[1]e-mail: s.k.wilson@strath.ac.uk
[2]e-mail: b.r.duffy@strath.ac.uk

absent from Hartley and Murgatroyd's [1] theoretical analysis. This analysis was extended by Murgatroyd [4] to include the effects of surface shear stress and 'form drag' due to the presence of a gas stream above the fluid film. Wilson [5] developed a more sophisticated model for the flow which assumes that the cross-section of the capillary ridge is a circular arc. Podgorski *et al.* [3] independently developed a model similar to that of Wilson [5] based on a balance between surface-tension forces and the weight of the capillary ridge, and found good agreement between their theoretical predictions and experimental measurements. Recently, Wilson *et al.* [6] obtained similarity solutions describing a slender dry patch in a gravity-driven film for the cases of both strong gravitational and strong surface-tension effects. When gravitational effects are strong the dry patch has a parabolic shape and the transverse profile of the free surface has a monotonically increasing shape. When surface-tension effects are strong the dry patch has a quartic shape and the transverse profile of the free surface has a capillary ridge near the contact line and decays in an oscillatory manner far from it.

There has also been some work done on dry patches in non-isothermal films. Zuber and Staub [7] extended Hartley and Murgatroyd's [1] analysis to include both thermocapillarity and vapour thrust. McPherson [8] further included the hydrostatic head and the form drag introduced by Murgatroyd [4], but concluded that both effects are insignificant. Later Chung and Bankoff [9] extended the approach of Zuber and Staub [7] to include the hydrostatic head and a non-zero shear stress on the solid substrate.

In this paper we follow the approach of Wilson *et al.* [6] and use the lubrication approximation to investigate slender dry patches in an infinitely wide thin film of viscous fluid flowing steadily on an inclined plane that is either heated or cooled relative to the surrounding atmosphere. Four non-isothermal situations in which thermocapillary effects play a significant role are considered. Similarity solutions describing a thermocapillary-driven flow with a dry patch that is widening or narrowing due to either gravitational or surface-tension effects on a non-uniformly heated or cooled substrate are obtained. Similarity solutions are also obtained for a gravity-driven and a constant-surface-shear-stress-driven flow with a dry patch that is widening or narrowing due to thermocapillarity on a uniformly heated or cooled substrate. In each situation one or more solutions corresponding to widening and/or narrowing dry patches are obtained and analysed in detail. The present work is a companion to the paper by Holland *et al.* [10] who study the steady flow of slender rivulets on a heated or cooled inclined plane in the four analogous situations.

2. Problem formulation

We consider the steady flow of an infinitely wide thin film of viscous fluid around a symmetric slender dry patch on a heated or cooled plane inclined at an angle α ($0 \leq \alpha \leq \pi$) to the horizontal, when there is an imposed constant shear stress on the free surface and the surface tension of the fluid varies linearly with temperature. We consider both sessile dry patches (when $0 \leq \alpha < \pi/2$) and pendent dry patches (when $\pi/2 < \alpha \leq \pi$), as well as dry patches on a vertical substrate (when $\alpha = \pi/2$). Cartesian coordinates $Oxyz$ with the x-axis down the line of greatest slope and the z-axis normal to the substrate are adopted, with the substrate at $z = 0$. The edges of the dry patch are at $y = \pm y_{\mathrm{e}}(x)$. The geometry of the problem is shown in Figure 1.

Much of the formulation of the present problem follows that of Holland *et al.* [10] (also described by Holland [11]) and so only the most important details are reproduced here. The

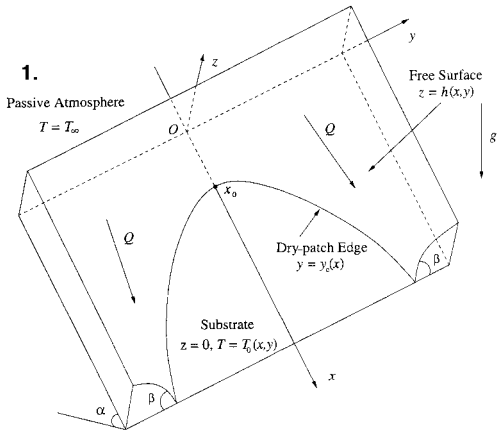

Figure 1. Geometry of the problem.

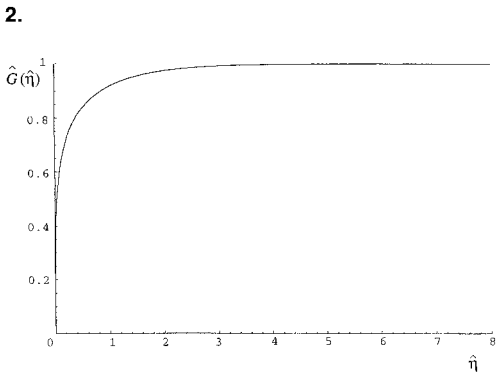

Figure 2. A thermocapillary-driven flow with a dry patch widening or narrowing due to gravity: the inner solution for the free-surface profile in the limit $G_\infty \to 0$, $\hat{G}(\hat{\eta})$, given by (35) plotted as a function of $\hat{\eta}$.

differences between the rivulet problem and the present dry-patch problem occur in the boundary conditions on the free surface $z = h(x, y)$ and in the appropriate definition of the volume flux Q. For both problems the surface tension $\gamma = \gamma(T)$ is assumed to depend linearly on temperature $T = T(x, y, z)$ according to

$$\gamma(T) = \gamma_\mathrm{r} - \lambda(T - T_\mathrm{r}), \tag{1}$$

where T_r is a reference temperature taken to be the temperature of the substrate at some position $x = x_0$, $y = 0$, γ_r is the surface tension when $T = T_\mathrm{r}$, and $\lambda = -\mathrm{d}\gamma/\mathrm{d}T$ is a positive constant. Note that T_r may be greater than or less than the prescribed uniform temperature of the passive atmosphere above the fluid, denoted by T_∞, corresponding to the substrate at $x = x_0$, $y = 0$ being hotter or colder than the atmosphere, respectively. The prescribed average volume flux around the dry patch per unit width in the transverse (*i.e.*, in the y) direction is given by

$$Q = \lim_{y\to\infty} y^{-1} \int_{y_\mathrm{e}}^{y} \int_{0}^{h} u \,\mathrm{d}z \,\mathrm{d}\tilde{y}, \tag{2}$$

where Q is a positive constant, and $u = u(x, y, z)$ is the fluid velocity in the longitudinal (*i.e.*, in the x) direction. At the edges of the dry patch $y = \pm y_\mathrm{e}$ where $h = 0$ a condition must be specified concerning the contact angle $\beta = \beta(x, y_\mathrm{e}(x))$. For example, β may be assumed to satisfy a fixed-contact-angle condition, or to depend on the substrate temperature in a prescribed way; however, for our purposes it is not necessary to be specific about this condition. Using the scalings adopted by Holland *et al.* [10], with $Q = \epsilon\delta l U$ in place of their definition of the longitudinal velocity scale U, where $\epsilon \ll 1$ and $\delta \ll 1$ are the longitudinal and transverse aspect ratios respectively (*i.e.*, the aspect ratios in the (x, z) and (y, z) planes, respectively) and l is the longitudinal length scale, we obtain the same non-dimensional governing partial differential equation for h (their Equation (36)), namely

$$\left[\frac{h^3}{3}\left\{S\cos\alpha h\ -\frac{1}{C}h_{yy}+\frac{\delta^2}{\epsilon^2\Delta C}\left(\frac{T_0}{1+Bh}-1\right)h_{yy}\right\}_y+\frac{1}{\epsilon^2\Delta C}\frac{h^2}{2}\left(\frac{T_0}{1+Bh}\right)_y\right]_y \\ -\left[\frac{\epsilon S\sin\alpha}{\delta}\frac{h^3}{3}+\tau\frac{h^2}{2}-\frac{1}{\Delta C}\frac{h^2}{2}\left(\frac{T_0}{1+Bh}\right)_x\right]_x=0, \tag{3}$$

together with the new non-dimensional flux condition (replacing their Equation (37)), namely

$$1=\lim_{y\to\infty}y^{-1}\int_{y_e}^{y}\left[\frac{\epsilon S\sin\alpha}{\delta}\frac{h^3}{3}+\tau\frac{h^2}{2}-\frac{1}{\Delta C}\frac{h^2}{2}\left(\frac{T_0}{1+Bh}\right)_x\right]\mathrm{d}\tilde{y}. \tag{4}$$

Here $T_0 = T_0(x, y)$ is the non-dimensional prescribed substrate temperature (which is, in general, a non-constant function of x and y), τ is the non-dimensional imposed constant shear stress on the free surface in the longitudinal (*i.e.*, in the (x, z)) plane, and the four non-dimensional parameters that arise are the Stokes number S, the capillary number C, the thermocapillary number ΔC and the Biot number B, defined by

$$S=\frac{\epsilon\delta^3\rho g l^2}{\mu U},\quad C=\frac{\epsilon\mu U}{\delta^3\gamma_r},\quad \Delta C=\frac{\mu U}{\epsilon\delta\lambda(T_r-T_\infty)},\quad B=\frac{\epsilon\delta\alpha_{th}l}{k_{th}}, \tag{5}$$

where ρ, μ and k_{th} are the constant density, viscosity and thermal conductivity of the fluid respectively, and α_{th} is the surface heat-transfer coefficient. Hereafter, unless it is stated otherwise, all quantities will be non-dimensional.

At the contact line $y = y_e(x)$ we have

$$h=0,\quad h_y=\beta, \tag{6}$$

and in the limit $y \to \infty$ we have

$$\lim_{y\to\infty}h=h_\infty, \tag{7}$$

where $h_\infty = h_\infty(x)$ is the thickness of the film far from the dry patch (which is, in general, a non-constant function of x). With (7) the flux condition (4) simplifies to

$$1=\frac{\epsilon S\sin\alpha}{\delta}\frac{h_\infty^3}{3}+\tau\frac{h_\infty^2}{2}-\frac{1}{\Delta C}\frac{h_\infty^2}{2}\lim_{y\to\infty}y^{-1}\int_{y_e}^{y}\left(\frac{T_0}{1+Bh}\right)_x\mathrm{d}\tilde{y}. \tag{8}$$

In the special case in which the substrate temperature is independent of y (*i.e.*, when $T_0 = T_0(x)$) the flux condition (8) simplifies further to

$$1=\frac{\epsilon S\sin\alpha}{\delta}\frac{h_\infty^3}{3}+\tau\frac{h_\infty^2}{2}-\frac{1}{\Delta C}\frac{h_\infty^2}{2}\left(\frac{T_0}{1+Bh_\infty}\right)_x. \tag{9}$$

Equations (3) and (8) are rather general equations for a slender dry patch in an infinitely wide film subject to gravity, surface tension, thermocapillarity and a constant surface shear stress. Particular forms of these equations have been studied previously for isothermal flow by Wilson *et al.* [6] who considered a dry patch in a gravity-driven film for the cases of both strong gravitational and strong surface-tension effects. In the case of strong gravitational effects the two gravity terms in (3) (that is, the terms in S) are dominant with the gravity term dominating the flux condition (9). In the case of strong surface-tension effects the dominant balance in (3) is between surface tension (represented by the term in $1/C$) and gravity (represented by the term in $S\sin\alpha$), with gravity again dominating the flux condition (9).

Following the approach of Wilson *et al.* [6] we seek similarity solutions of (3) and (9) for h of the form

$$h = bf(x)G(\eta), \quad \eta = \frac{y}{y_e(x)}, \tag{10}$$

in which the constant b (included for convenience) and the functions $f = f(x)$, $y_e = y_e(x)$ and $G = G(\eta)$ are to be determined, where G satisfies the contact-line condition

$$G(1) = 0 \tag{11}$$

and the far-field condition

$$\lim_{\eta\to\infty} G(\eta) = G_\infty, \tag{12}$$

where G_∞ is a constant satisfying $h_\infty(x) = bf(x)G_\infty$. Solutions of the form (10) cannot, in general, satisfy a prescribed contact-angle condition of the type discussed earlier. The isothermal dry-patch similarity solutions obtained by Wilson *et al.* [6] and the isothermal rivulet similarity solutions obtained by Smith [12] and Duffy and Moffatt [13] have similar shortcomings. Wilson *et al.* [6] showed how the isothermal rivulet solutions can be modified locally near the contact line to accommodate a fixed-contact-angle condition by incorporating sufficiently strong slip at the solid/fluid interface into the model. Unfortunately, this procedure does not work for the isothermal dry-patch solutions and so is not attempted here. Evidently we must have $y_e \geq 0$ and $h \geq 0$ for the solution (10) to be physically relevant, and without loss of generality we therefore take b, f and G_∞ to be positive and y_e and G to be non-negative. In the sections that follow x_0 (which may be infinite) is chosen such that $y_e(x_0) = 0$, and solutions in both $x \leq x_0$ and $x \geq x_0$ will be considered.

3. Thermocapillary-driven flow with a dry patch widening or narrowing due to gravity

In this section we consider thermocapillary-driven flow with a dry patch that is widening or narrowing due to gravity (*i.e.*, the case in which the first and last terms dominate (3) and the thermocapillary term dominates (9)). We consider a rather general non-uniform substrate-temperature distribution that depends on x but is independent of y, *i.e.*, $T_0 = T_0(x)$. For later convenience we write T_0 in the form

$$T_0 = 1 - \int_{x_0}^{x} \theta(\tilde{x})\,\mathrm{d}\tilde{x}, \tag{13}$$

satisfying $T_0(x_0) = 1$, $T_{0,x} = -\theta$ and $T_{0,y} = 0$, where $\theta = \theta(x)$ is a prescribed function of x. Setting $S|\cos\alpha| = 1/|\Delta C| = 1$, we find that ϵ, δ and U are given by

$$\epsilon = \left(\frac{\rho g|\cos\alpha|Q\mu l}{\lambda^2(T_\mathrm{r} - T_\infty)^2}\right)^{\frac{1}{2}} \ll 1, \quad \delta = \left(\frac{\lambda|T_\mathrm{r} - T_\infty|}{\rho g|\cos\alpha|l^2}\right)^{\frac{1}{2}} \ll 1, \quad U = \left(\frac{\lambda|T_\mathrm{r} - T_\infty|Q}{\mu l}\right)^{\frac{1}{2}}. \tag{14}$$

The remaining terms in (3) and (9) are negligible provided that

$$\frac{1}{C} \ll 1, \quad B \ll \epsilon^2, \quad \tau \ll 1, \quad |\tan\alpha| \ll \frac{\delta}{\epsilon}, \quad \frac{\delta^2}{\epsilon^2} \ll 1, \tag{15}$$

which, in particular, mean that surface tension, surface heat transfer and surface shear stress must be sufficiently small, and that $\alpha \ll 1$ or $\pi - \alpha \ll 1$ (so that the substrate is horizontal or nearly horizontal). In this case the governing equations (3) and (9) reduce to

$$(h^3 h_y)_y - \frac{3\sigma_T \sigma_c}{2}(h^2\theta)_x = 0 \tag{16}$$

and

$$1 = \frac{\sigma_T \theta}{2} h_\infty^2 \tag{17}$$

at leading order, where we have written

$$\sigma_T = \mathrm{sgn}(T_r - T_\infty), \quad \sigma_c = \mathrm{sgn}(\cos\alpha), \tag{18}$$

so that $\sigma_T = \pm 1$ correspond to the substrate at $x = x_0$, $y = 0$ being hotter or colder than the surrounding atmosphere, respectively, and $\sigma_c = \pm 1$ correspond to a sessile or a pendent dry patch, respectively. Note that (17) requires $\sigma_T \theta > 0$; in particular, this means that θ must be of one sign.

Seeking a solution of (16), and (17) in the form (10), we have

$$(G^3 G')' - \frac{3\sigma_T \sigma_c}{2b^2}(C_1 G^2 - 2C_2 \eta G G') = 0 \tag{19}$$

and

$$1 = \frac{\sigma_T}{2} C_3 (bG_\infty)^2, \tag{20}$$

where

$$C_1 = \frac{(\theta f^2)' y_e^2}{f^4}, \quad C_2 = \frac{\theta y_e y_e'}{f^2}, \quad C_3 = \theta f^2 \neq 0 \tag{21}$$

are constants, and a prime denotes differentiation with respect to argument. Since C_3 is constant, we can deduce immediately that $(\theta f^2)' = 0$, and hence that $C_1 = 0$.

Equation (19) has the trivial solution $G = G_\infty$ which satisfies the far-field condition (12), but not the contact-line condition (11). However, we can truncate this solution at $|\eta| = 1$ to obtain the non-trivial solution

$$h = \left|\frac{2}{\theta}\right|^{\frac{1}{2}} \quad \text{for} \quad |y| \geq y_e, \tag{22}$$

where $y_e = y_e(x)$ is an arbitrary function, representing a dry patch of arbitrary width in an infinitely wide film whose transverse (but not, in general, longitudinal) profile is uniform.

In the general case $C_2 \neq 0$ the product of C_2 and C_3 in (21) leads to $(y_e^2)' = 2C_2 C_3 \theta^{-2}$. If we define the function $J = J(x)$ by

$$J = \int_{x_0}^{x} \theta(\tilde{x})^{-2}\, \mathrm{d}\tilde{x}, \tag{23}$$

then, provided that $C_2 C_3 J \geq 0$, we have

$$y_e = (2C_2 C_3 J)^{\frac{1}{2}}. \tag{24}$$

From C_3 in (21) we find that

$$f = \left(\frac{C_3}{\theta}\right)^{\frac{1}{2}}. \tag{25}$$

With the choice $b = |3C_2|^{1/2}$ Equation (19) reduces to

$$(G^3G')' + s\eta GG' = 0, \tag{26}$$

where $s = \sigma_T\sigma_c\mathrm{sgn}(C_2) = \mathrm{sgn}\left(\cos\alpha y_e'\right)$, and the flux condition (20) becomes

$$1 = \frac{3\sigma_T}{2}|C_2|C_3G_\infty^2. \tag{27}$$

In the special case $C_2 = 0$ the solution is given by (22) with y_e an arbitrary constant, representing a parallel-sided dry patch of arbitrary width in an infinitely wide film whose transverse (but not, in general, longitudinal) profile is uniform.

The exact solution of (26) that satisfies (11) and (12) has not been found; however, considerable analytical progress can still be made and the equation can be solved numerically.

3.1. Behaviour as $\eta \to 1^+$

Seeking a local solution of (26) near the contact line $\eta = 1$ in the form $G \sim a(\eta - 1)^r$, where a and r are real and positive constants, we find that the local behaviour of G as $\eta \to 1^+$ is given either by

$$G = a(\eta - 1)^{\frac{3}{4}} - \frac{s}{3a}(\eta - 1)^{\frac{3}{4}} + o(\eta - 1)^{\frac{3}{4}} \tag{28}$$

for $s = \pm 1$, where $a > 0$ is an arbitrary constant, or by

$$G = (\eta - 1)^{\frac{1}{2}} + o(\eta - 1)^{\frac{1}{2}} \tag{29}$$

for $s = -1$ only. Both (28) and (29) imply that $G'(1) = \infty$ and hence the lubrication approximation fails near $\eta = 1$. There is no immediate reason for disregarding either (28) or (29); however, as we shall see shortly, there is no solution with the appropriate behaviour as $\eta \to \infty$ when $s = -1$, and so the local behaviour of G as $\eta \to 1^+$ is given by (28) with $s = 1$.

3.2. Behaviour as $\eta \to \infty$

As $\eta \to \infty$ we have $G \sim G_\infty$, and so writing $G = G_\infty + G_1(\eta)$ in (26) and linearising for small G_1 we obtain

$$G_\infty^2 G_1'' + s\eta G_1' = 0. \tag{30}$$

A solution for G_1 is possible only when $s = 1$; therefore, for the remainder of Section 3 we shall consider only the case $s = 1$. Equation (30) can be integrated directly to yield

$$G_1 = A\left(\frac{\pi}{2G_\infty^2}\right)^{\frac{1}{2}}\left[1 - \mathrm{erf}\left(\frac{\eta^2}{2G_\infty^2}\right)^{\frac{1}{2}}\right], \tag{31}$$

where A is an undetermined real constant. Therefore

$$G \sim G_\infty + A\eta^{-1}\exp\left(-\frac{\eta^2}{2G_\infty^2}\right) \tag{32}$$

as $\eta \to \infty$, and hence G approaches G_∞ monotonically in this limit.

3.3. THE SINGULAR LIMIT $G_\infty \to 0$

In the singular limit $G_\infty \to 0$ we write $G = G_\infty \widehat{G}(\eta)$ so that (26) becomes

$$G_\infty^2(\widehat{G}^3\widehat{G}')' + \eta\widehat{G}\widehat{G}' = 0. \tag{33}$$

In the limit $G_\infty \to 0$ the leading-order version of Equation (33) is $\widehat{G}' = 0$, and so the appropriate outer solution is simply $\widehat{G} = 1$. This outer solution fails near the contact line $\eta = 1$. In the inner region we introduce a rescaled coordinate defined by $\eta = 1 + G_\infty^2\hat{\eta}$, and hence (using the matching condition with the outer solution) at leading order (33) becomes

$$\widehat{G}' = \frac{1}{2}(\widehat{G}^{-3} - \widehat{G}^{-1}). \tag{34}$$

Solving (34) and using the contact-line condition $\widehat{G} = 0$ at $\hat{\eta} = 0$, we obtain the implicit solution

$$\hat{\eta} = -\left[\widehat{G}^2 + \log(1 - \widehat{G}^2)\right], \tag{35}$$

which is shown in Figure 2. Since the leading-order outer solution is a constant, the uniformly valid leading-order composite solution is simply

$$G = G_\infty \widehat{G}\left(\frac{\eta - 1}{G_\infty^2}\right). \tag{36}$$

In particular, in the limit $\eta \to 1^+$ this solution satisfies

$$G = (2G_\infty^2)^{\frac{1}{4}}(\eta - 1)^{\frac{1}{4}} - \frac{1}{3(2G_\infty^2)^{\frac{1}{4}}}(\eta - 1)^{\frac{3}{4}} + o(\eta - 1)^{\frac{3}{4}}, \tag{37}$$

which coincides with (28) up to the order shown, provided that $a = (2G_\infty^2)^{1/4}$ and $s = 1$. Moreover, in the limit $\eta \to \infty$ we have

$$G \sim G_\infty - \frac{G_\infty}{2}\exp\left(-1 + \frac{1}{G_\infty^2}\right)\exp\left(-\frac{\eta}{G_\infty^2}\right); \tag{38}$$

this differs somewhat from (32), but shows that G still approaches G_∞ monotonically in this limit.

3.4. NUMERICAL SOLUTION

We solved the system (11), (12) and (26) numerically, using an Adams method implemented by the computer algebra package *Mathematica*. It was found that a real and positive solution for G is possible only when $s = 1$ (which is consistent with Section 3.2).

The numerical calculations were started from $\eta = 1 + \zeta$ for sufficiently small $\zeta \ll 1$ by using (28) to give the approximate initial conditions

$$G(1 + \zeta) = a\zeta^{\frac{1}{4}} - \frac{1}{3a}\zeta^{\frac{3}{4}}, \quad G'(1 + \zeta) = \frac{a}{4}\zeta^{-\frac{3}{4}} - \frac{1}{4a}\zeta^{-\frac{1}{4}}. \tag{39}$$

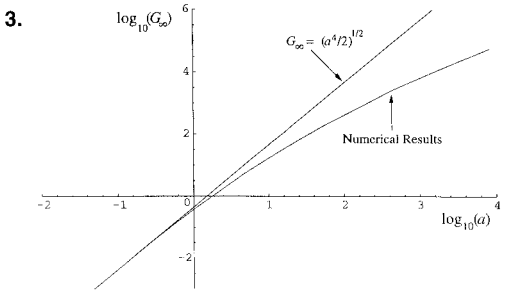

Figure 3. Numerically calculated values of $\log_{10}(G_\infty)$ obtained in Section 3.4 plotted as a function of $\log_{10}(a)$ together with the leading-order asymptotic value of G_∞ in the limit $G_\infty \to 0$, namely $G_\infty = (a^4/2)^{1/2}$.

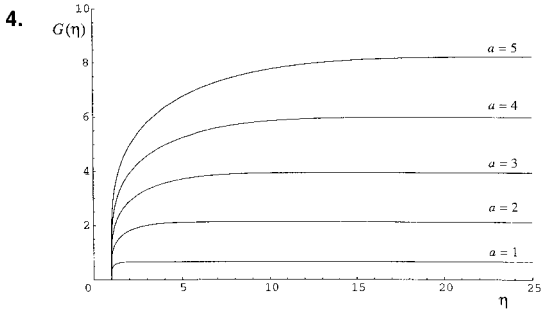

Figure 4. Numerically calculated free-surface profiles $G(\eta)$ obtained in Section 3.4 plotted as a function of η for $a = 1, 2, \ldots, 5$.

Equation (26) was integrated forwards in η for a range of values of a. In all the cases investigated the solutions obtained approach a limiting value as $\eta \to \infty$, and hence the relationship between a and G_∞ was determined. Figure 3 shows this relationship, and compares it with the leading-order asymptotic solution in the limit $G_\infty \to 0$ calculated in Section 3.3, namely $G_\infty = (a^4/2)^{1/2}$; clearly there is excellent agreement for sufficiently small values of G_∞. Typical free-surface profiles are shown in Figure 4 for a range of values of a. Note that all the free-surface profiles in Figure 4 have a monotonically increasing shape.

3.5. Solution for h in the case $C_2 \neq 0$

The solution in the general case $C_2 \neq 0$ takes the form

$$h = \left|\frac{2}{\theta G_\infty^2}\right|^{\frac{1}{2}} G\left(\frac{y}{y_e}\right), \quad y_e = \left|\frac{4J}{3G_\infty^2}\right|^{\frac{1}{2}}, \tag{40}$$

where G satisfies (26), which is valid, provided that $s = \mathrm{sgn}(\cos\alpha(x - x_0)) = 1$. The solution (40) is unique for each value of G_∞; this solution represents both a narrowing ($y_e' < 0$) pendent ($\cos\alpha < 0$) dry patch in $x \leq x_0$, and a widening ($y_e' > 0$) sessile ($\cos\alpha > 0$) dry patch in $x \geq x_0$. Provided that $\theta(x_0)$ is finite and non-zero for $|x_0| < \infty$, we have $J = O(x - x_0)$ as $x \to x_0$, and hence $y_e = O(|x - x_0|^{1/2})$ in this limit.

From (14) and (15) the conditions for this solution to be valid can be expressed as $\epsilon \ll 1$, $\delta \ll 1$,

$$\begin{gathered}\left(\frac{\lambda^2(T_r - T_\infty)^2\gamma_r}{(\rho g\cos\alpha)^2 Q\mu}\right)^{\frac{1}{3}} \ll l, \quad \frac{\alpha_{th}^2\lambda^3|T_r - T_\infty|^3}{k_{th}^2(\rho g\cos\alpha)^2 Q\mu} \ll l, \quad l \ll \frac{\lambda|T_r - T_\infty|}{\tau}, \\ l \ll \left(\frac{\lambda^3|T_r - T_\infty|^3}{(\rho g\cos\alpha)^2\tan^2\alpha\, Q\mu}\right)^{\frac{1}{3}}, \quad \left(\frac{\lambda^3|T_r - T_\infty|^3}{(\rho g\cos\alpha)^2 Q\mu}\right)^{\frac{1}{3}} \ll l.\end{gathered} \tag{41}$$

We proceed by giving the details of this solution for a particular choice of the substrate-temperature gradient. As a simple example we consider a power-law substrate-temperature gradient with $\theta = x^k$, where k is a constant. Considering solutions for $x \geq 0$ (so that $\theta \geq 0$ and $x_0 \geq 0$), we have from (23)

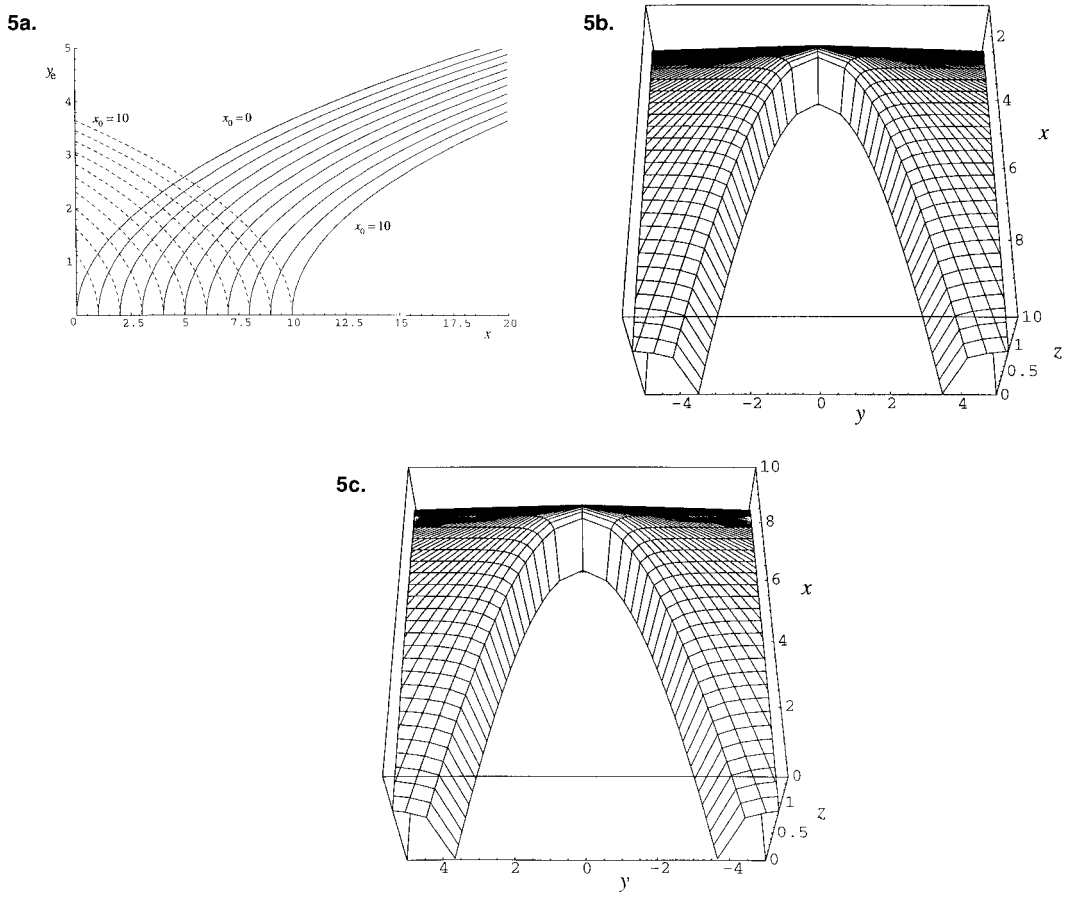

Figure 5. (a) Solutions for y_e from (40) in the case $\theta = 1$ for $x_0 = 0, 1, \ldots, 10$ showing both narrowing ($y_e' < 0$) pendent ($\cos\alpha < 0$) dry patches in $x \leq x_0$ (represented by the dashed lines), and widening ($y_e' > 0$) sessile ($\cos\alpha > 0$) dry patches in $x \geq x_0$ (represented by the solid lines), together with numerically calculated three-dimensional plots of the solution h given by (40) in (b) the sessile case when $x_0 = 1$, and (c) the pendent case when $x_0 = 10$. Note that the direction of flow is from top to bottom in (b), but from bottom to top in (c). Furthermore, note that for the particular choice $\theta = 1$ (but *not* in general otherwise) the solution in the pendent case is a reflection of that in the sessile case.

$$J = \begin{cases} \dfrac{x^{1-2k} - x_0^{1-2k}}{1-2k} & k \neq \dfrac{1}{2}, \\ \log\dfrac{x}{x_0} & k = \dfrac{1}{2}. \end{cases} \tag{42}$$

Evidently a solution with $x_0 = 0$ is possible only for $k < 1/2$, and a solution with $x_0 = \infty$ is possible only for $k > 1/2$. In the general case $k \neq 1/2$ the solution (40) is

$$h = \left(\frac{2}{x^k G_\infty^2}\right)^{\frac{1}{2}} G\left(\frac{y}{y_e}\right), \quad y_e = \left|\frac{4(x^{1-2k} - x_0^{1-2k})}{3(1-2k)G_\infty^2}\right|^{\frac{1}{2}}, \tag{43}$$

and in the special case $k = 1/2$ it is

$$h = \left(\frac{4}{xG_\infty^4}\right)^{\frac{1}{4}} G\left(\frac{y}{y_e}\right), \quad y_e = \left|\frac{4\log x/x_0}{3G_\infty^2}\right|^{\frac{1}{2}}, \tag{44}$$

both of which are valid, provided that $s = 1$. In particular, in the special case of a uniform temperature gradient $\theta = 1$ (that is, when $k = 0$), we find from (43) that $y_e = 2\left(|x - x_0|/3G_\infty^2\right)^{1/2}$ and $h \to 2^{1/2}$ as $|y| \to \infty$, so that the film is of uniform thickness far from the dry patch.

Figures 5–7 show the solutions for y_e and h in cases with $k = 0$ ($< 1/2$), $k = 1/2$ and $k = 1$ ($> 1/2$), respectively, for a range of values of x_0. These figures show both narrowing ($y_e' < 0$) pendent ($\cos\alpha < 0$) dry patches in $x \le x_0$ (represented by the dashed lines in the figures for y_e), and widening ($y_e' > 0$) sessile ($\cos\alpha > 0$) dry patches in $x \ge x_0$ (represented by the solid lines in the figures for y_e). As the figures show, for $x_0 > 0$ we have $y_e = O(1)$ as $x \to 0^+$ when $k < 1/2$, and $y_e = O(x^n)$ as $x \to 0^+$ when $k > 1/2$, where $n = (1 - 2k)/2$. On the other hand, for $x_0 = 0$ (in which case $k < 1/2$) we have $y_e = O(x^n)$ as $x \to 0^+$. Moreover, for $x_0 < \infty$ we have $y_e = O(x^n)$ as $x \to \infty$ when $k < 1/2$, and $y_e = O(1)$ as $x \to \infty$ when $k > 1/2$. On the other hand, for $x_0 = \infty$ (in which case $k > 1/2$) we have $y_e = O(x^n)$ as $x \to \infty$. In the special case $k = 1/2$ for $0 < x_0 < \infty$ we have $y_e = O(|\log x|^{1/2})$ both as $x \to 0^+$ and as $x \to \infty$.

Holland [11] gives details of the solution (40) for two further choices of the substrate-temperature gradient, namely an exponential temperature gradient and a spatially periodic temperature gradient.

4. Thermocapillary-driven flow with a dry patch widening or narrowing due to surface tension

In this section we consider thermocapillary-driven flow with a dry patch that is widening or narrowing due to surface tension (*i.e.*, the case in which the second and last terms dominate (3) and the thermocapillary term dominates (9)). As in Section 3, the substrate-temperature distribution is taken to be in the form (13). Setting $C = |\Delta C| = 1$, we find that ϵ, δ and U are given by

$$\epsilon = \left(\frac{\gamma_r Q\mu}{\lambda^2(T_r - T_\infty)^2 l}\right)^{\frac{1}{4}} \ll 1, \quad \delta = \left(\frac{Q\mu}{\gamma_r l}\right)^{\frac{1}{4}} \ll 1, \quad U = \left(\frac{\lambda|T_r - T_\infty|Q}{\mu l}\right)^{\frac{1}{2}}. \tag{45}$$

The remaining terms in (3) and (9) are negligible, provided that

$$\frac{\epsilon S \sin\alpha}{\delta} \ll 1, \quad S|\cos\alpha| \ll 1, \quad B \ll \epsilon^2, \quad \tau \ll 1, \quad \frac{\delta^2}{\epsilon^2} \ll 1, \tag{46}$$

which, in particular, mean that gravity, surface heat transfer and surface shear stress must be sufficiently small; however, unlike in the case considered in Section 3, there is no restriction on α and so solutions are valid for $0 \le \alpha \le \pi$. In this case the governing Equations (3) and (9) reduce to

$$(h^3 h_{yyy})_y + \frac{3\sigma_T}{2}(h^2\theta)_x = 0 \tag{47}$$

and (17) at leading order, where σ_T is given by (18). As in Section 3, θ must be of one sign.

Seeking a solution of (47) and (17) in the form (10) we have

$$(G^3 G''')' + \frac{3\sigma_T}{2b^2}(C_4 G^2 - 2C_5\eta G G') = 0 \tag{48}$$

and (20), where

6a.

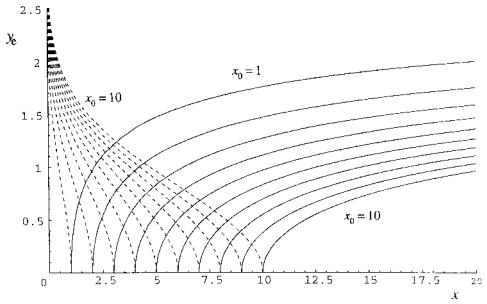

6b.

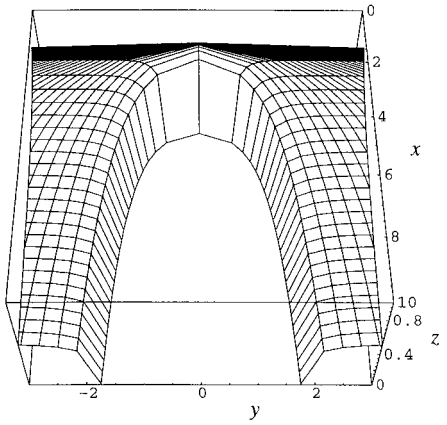

6c.

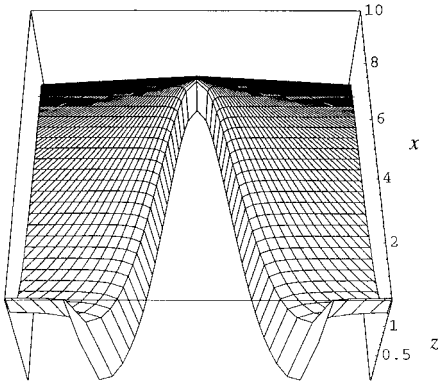

Figure 6. As for Figure 5 except that $\theta = x^{1/2}$ and (a) is exclusive of $x_0 = 0$.

7a.

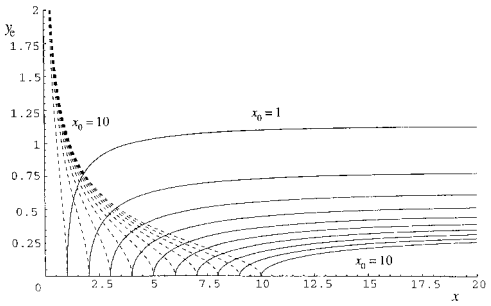

7b.

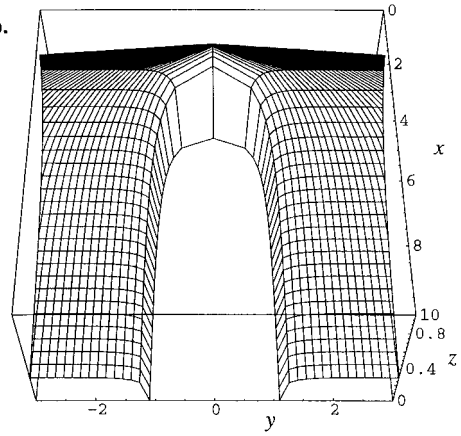

7c.

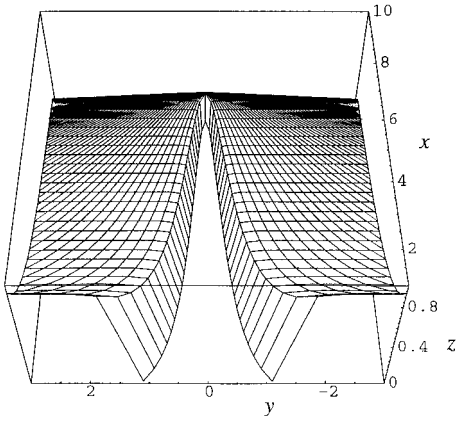

Figure 7. As for Figure 5 except that $\theta = x$ and (a) is exclusive of $x_0 = 0$.

$$C_4 = \frac{(\theta f^2)' y_e^4}{f^4}, \quad C_5 = \frac{\theta y_e^3 y_e'}{f^2} \tag{49}$$

are constants. As in Section 3, we can deduce immediately that $C_4 = 0$.

Also, as in Section 3, Equation (48) has the trivial solution $G = G_\infty$ which satisfies the far-field condition (12) but not the contact-line condition (11). However, we can again truncate this solution at $|\eta| = 1$ to obtain the non-trivial solution (22), where $y_e = y_e(x)$ is an arbitrary function.

In the general case $C_5 \neq 0$ the product of C_3 in (21) and C_5 in (49) leads to $(y_e^4)' = 4C_3C_5\theta^{-2}$. Provided that $C_3C_5J \geq 0$ (where the function $J = J(x)$ is defined by (23)), we have

$$y_e = (4C_3C_5J)^{\frac{1}{4}}. \tag{50}$$

From C_3 in (21) we again find that f is given by (25). With the choice $b = |3C_5|^{1/2}$ Equation (48) reduces to

$$(G^3G''')' - s\eta GG' = 0, \tag{51}$$

where $s = \sigma_T \mathrm{sgn}(C_5) = \mathrm{sgn}(y_e')$, and the flux condition (20) becomes

$$1 = \frac{3\sigma_T}{2} C_3 |C_5| G_\infty^2. \tag{52}$$

In the special case $C_5 = 0$ the solution is again given by (20) with y_e an arbitrary constant.

As in Section 3, the exact solution of (51) that satisfies (11) and (12) has not been found; however, again considerable analytical progress can still be made and the equation can be solved numerically.

4.1. Behaviour as $\eta \to 1^+$

The local behaviour of G as $\eta \to 1^+$ is given either by

$$G = a(\eta - 1)^{\frac{3}{4}} + \frac{16s}{45a}(\eta - 1)^{\frac{9}{4}} + o(\eta - 1)^{\frac{9}{4}} \tag{53}$$

or by

$$G = a(\eta - 1) + \frac{s}{4a}(\eta - 1)^2[\log(\eta - 1) + a_0] + o(\eta - 1)^2 \tag{54}$$

for $s = \pm 1$, where $a > 0$ and a_0 are arbitrary constants, or by

$$G = \frac{2}{\sqrt{3}}(\eta - 1)^{\frac{3}{2}} + o(\eta - 1)^{\frac{3}{2}} \tag{55}$$

for $s = -1$ only. Note that (53) (but not (54) or (55)) implies that $G'(1) = \infty$ and hence the lubrication approximation fails near $\eta = 1$ in that case. As in Section 3.1, there is no immediate reason for disregarding any of the solutions (53)–(55); however, as we shall see subsequently, the present numerical results indicate that the behaviour is described by (53).[1]

4.2. Behaviour as $\eta \to \infty$

As $\eta \to \infty$ we have $G \sim G_\infty$, and so, writing $G = G_\infty + G_1$ in (51) and linearising for small G_1, we obtain

[1]Note that there is an omission from the corresponding results in [6] for an isothermal gravity-driven dry patch with strong surface-tension effects, which we rectify in the Appendix.

$$G_\infty^2 G_1'''' - s\eta G_1' = 0. \tag{56}$$

The exact solution of (56) can be found in terms of hypergeometric functions, but is not particularly informative. However, information about the behaviour of G_1 in the limit $\eta \to \infty$ can be obtained by seeking a solution in the form $G_1 \sim A_0 \eta^p \exp(-A_1 \eta^q)$, where the complex constants A_0 and A_1 (with $\mathfrak{Re}(A_1) > 0$) and the real exponents p and $q > 0$ are to be determined. Substituting this solution in (56) yields

$$A_1 = \frac{3}{8G_\infty^{\frac{2}{3}}}(1 \pm \sqrt{3}\mathrm{i}), \quad p = -\frac{2}{3}, \quad q = \frac{4}{3} \tag{57}$$

for $s = 1$, and

$$A_1 = \frac{3}{4G_\infty^{\frac{2}{3}}}, \quad p = -\frac{2}{3}, \quad q = \frac{4}{3} \tag{58}$$

for $s = -1$, but leaves A_0 undetermined in both cases. Thus, in the limit $\eta \to \infty$, we have

$$G \sim G_\infty + A\eta^{-\frac{2}{3}} \exp\left[-\frac{3}{8G_\infty^{\frac{2}{3}}}\eta^{\frac{4}{3}}\right] \cos\left[\frac{3\sqrt{3}}{8G_\infty^{\frac{2}{3}}}\eta^{\frac{4}{3}} + \phi\right] \tag{59}$$

for $s = 1$, and

$$G \sim G_\infty + A\eta^{-\frac{2}{3}} \exp\left[-\frac{3}{4G_\infty^{\frac{2}{3}}}\eta^{\frac{4}{3}}\right] \tag{60}$$

for $s = -1$, where A is an undetermined real constant and ϕ is an undetermined phase shift in the interval $[0, \pi)$, and hence in the case $s = 1$, G approaches G_∞ in an oscillatory manner, while in the case $s = -1$, G approaches G_∞ monotonically.

4.3. The singular limit $G_\infty \to 0$

In the singular limit $G_\infty \to 0$ we write $G = G_\infty \widehat{G}$ so that (51) becomes

$$G_\infty^2(\widehat{G}^3\widehat{G}''')' - s\eta\widehat{G}\widehat{G}' = 0. \tag{61}$$

In the limit $G_\infty \to 0$ the leading-order version of Equation (61) is again $\widehat{G}' = 0$, and so the appropriate outer solution is simply $\widehat{G} = 1$. As in Section 3.3, this outer solution fails near the contact line $\eta = 1$. In the inner region we introduce a rescaled coordinate defined by $\eta = 1 + G_\infty^{2/3}\hat{\eta}$, and hence at leading order (61) becomes

$$\widehat{G}''' = \frac{s}{2}(\widehat{G}^{-1} - \widehat{G}^{-3}). \tag{62}$$

Unlike for the corresponding equation in Section 3.3, we have been unable to find an exact solution to this equation that satisfies the contact-line condition $\widehat{G} = 0$ at $\hat{\eta} = 0$.

In the case $s = 1$ seeking a solution of (62) near $\hat{\eta} = 0$ in the form $\widehat{G} \sim a\hat{\eta}^r$ requires that $r = 3/4$ (in agreement with (53)) and $a = (-32/15)^{1/4}$ (which is complex), suggesting that there may be no solution to the problem in this limit in this case. This tentative conclusion is confirmed by the present numerical results.

In the case $s = -1$ the local behaviour of $\widehat{G}$ as $\hat{\eta} \to 0$ is given by

$$\widehat{G} = \left(\frac{32}{15}\right)^{\frac{1}{4}} \hat{\eta}^{\frac{3}{4}} - \frac{16}{45}\left(\frac{32}{15}\right)^{-\frac{1}{4}} \hat{\eta}^{\frac{9}{4}} + o(\hat{\eta}^{\frac{9}{4}}). \tag{63}$$

The uniformly valid leading-order composite solution is simply

$$G = G_\infty \widehat{G}\left(\frac{\eta - 1}{G_\infty^{\frac{2}{3}}}\right). \tag{64}$$

In particular, in the limit $\eta \to 1^+$ this solution satisfies

$$G = \left(\frac{32G_\infty^2}{15}\right)^{\frac{1}{4}}(\eta-1)^{\frac{3}{4}} - \frac{16}{45}\left(\frac{32G_\infty^2}{15}\right)^{-\frac{1}{4}}(\eta-1)^{\frac{9}{4}} + o(\eta-1)^{\frac{9}{4}}, \tag{65}$$

which coincides with (53) up to the order shown provided that $a = (32G_\infty^2/15)^{1/4}$ and $s = -1$. There are no solutions in this limit that correspond to either (54) or (55). Moreover, in the limit $\eta \to \infty$ we have

$$G \sim G_\infty + A\exp\left(-\frac{\eta}{G_\infty^{\frac{2}{3}}}\right), \tag{66}$$

where A is an undetermined real constant; this differs somewhat from (60), but shows that G still approaches G_∞ monotonically in this limit.

4.4. Numerical solution in the case $s = 1$

The system (11), (12) and (51) in the case when $s = 1$ was solved numerically using the method described in section 3.4. The first numerical calculations were started from $\eta = 1 + \zeta$ for sufficiently small $\zeta \ll 1$ by using (53) and (54) to give approximate initial conditions. However, neither (53) nor (54) yielded solutions for G that approach a limiting value as $\eta \to \infty$, as required; therefore all the numerical calculations presented here were instead calculated by integrating backwards in η from $\eta = X$ for sufficiently large $X \gg 1$, and using (59) to give the approximate initial conditions

$$\begin{aligned}
G(X) &= G_\infty + AX^{-\frac{2}{3}}\exp(-A_{1r}X^{\frac{4}{3}})\mathrm{C}_\phi,\\
G'(X) &= A\left(-\frac{4}{3}\right)X^{-\frac{1}{3}}\exp(-A_{1r}X^{\frac{4}{3}})(A_{1r}\mathrm{C}_\phi + A_{1i}\mathrm{S}_\phi),\\
G''(X) &= A\left(-\frac{4}{3}\right)^2\exp(-A_{1r}X^{\frac{4}{3}})[(A_{1r}^2 - A_{1i}^2)\mathrm{C}_\phi + 2A_{1r}A_{1i}\mathrm{S}_\phi],\\
G'''(X) &= A\left(-\frac{4}{3}\right)^3 X^{\frac{1}{3}}\exp(-A_{1r}X^{\frac{4}{3}})[(A_{1r}^2 - 3A_{1i}^2)A_{1r}\mathrm{C}_\phi + (3A_{1r}^2 - A_{1i}^2)A_{1i}\mathrm{S}_\phi],
\end{aligned} \tag{67}$$

where $A_1 = A_{1r} + \mathrm{i}A_{1i}$ is defined in (57), $\mathrm{C}_\phi = \cos(A_{1i}X^{4/3} + \phi)$ and $\mathrm{S}_\phi = \sin(A_{1i}X^{4/3} + \phi)$. The solutions calculated in this manner do not, in general, satisfy the contact-line condition (11), and indeed in some cases solutions do not even have a contact line.

Figure 8 shows numerically calculated solutions for G plotted as a function of η for several values of A in the case when $\phi = 0$ and $G_\infty = 1$. The present numerical results reveal that for $A > A_\mathrm{c} \simeq -3{\cdot}77$ the solutions do not have a contact line and diverge as $\eta \to -\infty$, while for $A \leq A_\mathrm{c}$ they have a contact line at $\eta = \eta^*$ which, in general, does not equal unity. When $A = A_\mathrm{c}$ it is found that $\eta^* \simeq 0{\cdot}878$, and decreasing A increases η^* until a maximum value of $\eta^* \simeq 0{\cdot}884$ is reached when $A \simeq -4{\cdot}04$, after which η^* decreases as A

8.

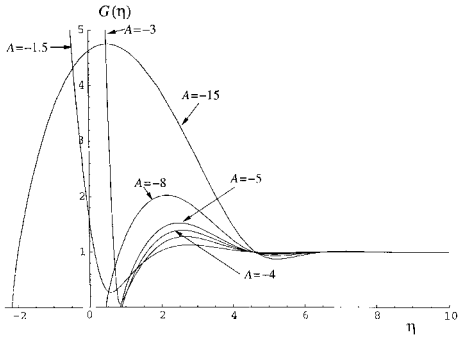

Figure 8. A thermocapillary-driven flow with a dry patch widening or narrowing due to surface tension: numerically calculated free-surface profiles $G(\eta)$ obtained in Section 4.4 plotted as a function of η when $s = 1$, $\phi = 0$, $G_\infty = 1$ for $A = -1{\cdot}5, -3, -4, -5, -8$ and -15. Note that none of the profiles shown have a contact line at $\eta = 1$ (and indeed those in the cases $A = -1{\cdot}5$ and -3 do not have a contact line at all).

9.

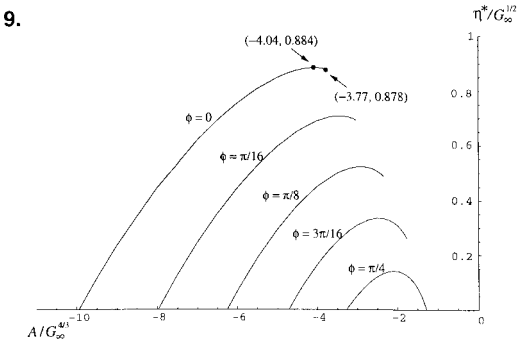

Figure 9. Numerically calculated values of the scaled contact-line position $\eta^*/G_\infty^{1/2}$ obtained in Section 4.4 plotted as a function of $A/G_\infty^{4/3}$ for a range of values of ϕ.

decreases. Qualitatively similar behaviour occurs for other values of ϕ and this is summarised in Figure 9, in which we plot $\eta^*/G_\infty^{1/2}$ as a function of $A/G_\infty^{4/3}$ for a range of values of ϕ in the case $G_\infty = 1$. (The reason for scaling η^* and A with G_∞ in this way will become apparent shortly.) As Figure 9 shows, when ϕ is increased from zero the curves for η^* as a function of A for fixed ϕ move downwards, and for sufficiently large values of ϕ satisfying $\phi > \phi_c \simeq 0{\cdot}294\pi$, the values of η^* are negative for all values of A and therefore do not appear on Figure 9 at all. Figure 9 also shows that there is no combination of values of A and ϕ for which $\eta^* = 1$, and therefore we deduce that there is no solution satisfying $G(1) = 0$ in the case $G_\infty = 1$. However, there are solutions that satisfy $G(1) = 0$ for larger values of G_∞, and Figure 9 contains all the information we need about the solutions when $G_\infty \neq 1$. To understand this we write

$$G(\eta) = G_\infty \bar{G}(\bar{\eta}), \quad \eta = G_\infty^{\frac{1}{2}}\bar{\eta}, \quad A = G_\infty^{\frac{4}{3}}\bar{A}, \tag{68}$$

where $\bar{G} = \bar{G}(\bar{\eta})$ is exactly the solution of the problem in the case $G_\infty = 1$ described above with $\bar{A}$ in place of A. Thus plotting $\eta^*/G_\infty^{1/2}$ as a function of $A/G_\infty^{4/3}$, as we have done in Figure 9, gives the same curves for *all* values of G_∞. Inspection of Figure 9 shows that solutions with $\eta^* = 1$ are impossible if $G_\infty < G_{\infty c}$, where $G_{\infty c} \simeq (0{\cdot}884)^{-2} \simeq 1{\cdot}280$, but for $G_\infty \geq G_{\infty c}$ there are solutions for values of ϕ in the interval $[0, \phi_{\max}]$, where the value of $\phi_{\max}$ ($\leq \phi_c$) depends on G_∞. In particular, Figure 9 shows that when $\phi = 0$ there is no solution for $G_\infty = 1$ ($< G_{\infty c}$), two solutions in the case $G_\infty = 1{\cdot}285$ (which lies in the range $G_{\infty c} \leq G_\infty \leq (0{\cdot}878)^{-2} \simeq 1{\cdot}297$), and one solution in the case $G_\infty = 2$ ($> 1{\cdot}297$). These solutions are shown in Figure 10. Figure 9 also shows that when $G_\infty = 10$ ($> G_{\infty c}$) there is one solution with $\phi = 0$, $\phi = \pi/16$ and $\phi = \pi/8$, two solutions with $\phi = 3\pi/16$, but no solutions with $\phi = \pi/4$. These solutions are shown in Figure 11. All the solutions in Figures 10 and 11 have a characteristic capillary ridge near the contact line and decay in an oscillatory manner as $\eta \to \infty$.

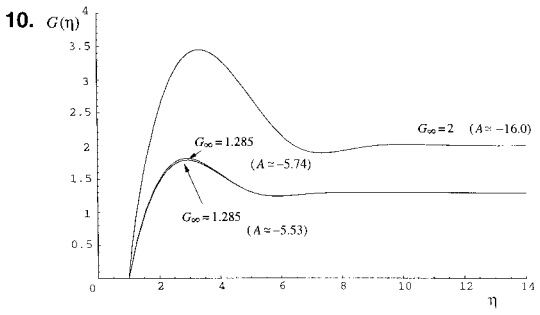

Figure 10. Numerically calculated free-surface profiles $G(\eta)$ obtained in Section 4.4 plotted as a function of η when $s = 1$ and $\phi = 0$ for $G_\infty = 1{\cdot}285$ (two almost identical solutions with $A \simeq -5{\cdot}53$ and $A \simeq -5{\cdot}74$, respectively) and $G_\infty = 2$ (one solution with $A \simeq -16{\cdot}0$).

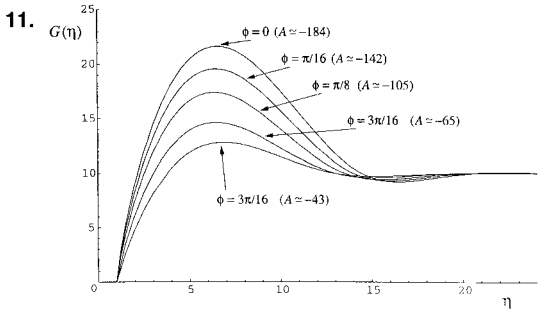

Figure 11. Numerically calculated free-surface profiles $G(\eta)$ obtained in Section 4.4 plotted as a function of η when $s = 1$ and $G_\infty = 10$ for $\phi = 0$ (one solution with $A \simeq -184$), $\phi = \pi/16$ (one solution with $A \simeq -142$), $\phi = \pi/8$ (one solution with $A \simeq -105$) and $\phi = 3\pi/16$ (two solutions with $A \simeq -43$ and $A \simeq -65$, respectively).

4.5. Numerical solution in the case $s = -1$

The system (11), (12) and (51) in the case when $s = -1$ was solved numerically using the method described in Section 4.4. In this case (60) was used to give the approximate initial conditions

$$G(X) = G_\infty + AX^{-\frac{2}{3}}\exp(-A_1X^{\frac{4}{3}}), \quad G'(X) = A\left(-\frac{4A_1}{3}\right)X^{-\frac{1}{3}}\exp(-A_1X^{\frac{4}{3}}),$$
$$G''(X) = A\left(-\frac{4A_1}{3}\right)^2\exp(-A_1X^{\frac{4}{3}}), \quad G'''(X) = A\left(-\frac{4A_1}{3}\right)^3X^{\frac{1}{3}}\exp(-A_1X^{\frac{4}{3}}), \tag{69}$$

where A_1 is defined in (58). With these initial conditions the equation can be integrated backwards in η and the value of A varied until the calculated position of the contact line where $G = 0$ is sufficiently close to $\eta = 1$. Equation (53) was used to calculate the corresponding value of a, and thus the relationship between a and G_∞ determined. Figure 12 shows this relationship, and compares it with the leading-order asymptotic solution in the limit $G_\infty \to \infty$ calculated in Section 4.3, namely $G_\infty = (15a^4/32)^{1/2}$; clearly there is excellent agreement for sufficiently small values of G_∞. Typical free-surface profiles are shown in Figure 13 for a range of values of G_∞. Note that all the free-surface profiles in Figure 13 have a monotonically increasing shape.

4.6. Solution for h in the case $C_5 \neq 0$

The solution in the general case $C_5 \neq 0$ takes the form

$$h = \left|\frac{2}{\theta G_\infty^2}\right|^{\frac{1}{2}} G\left(\frac{y}{y_e}\right), \quad y_e = \left|\frac{8J}{3G_\infty^2}\right|^{\frac{1}{4}}, \tag{70}$$

where G satisfies (51), which is valid for both $s = 1$ and $s = -1$, where $s = \mathrm{sgn}(x - x_0)$. In the case $s = 1$ there is no solution when $G_\infty < G_{\infty c} \simeq 1{\cdot}280$, but for $G_\infty \geq G_{\infty c}$ Equation (70) represents a one-parameter family of solutions (parameterised by ϕ). In the

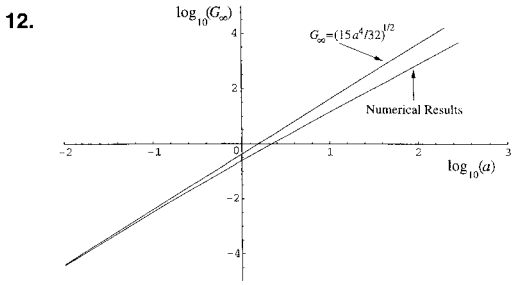

Figure 12. Numerically calculated values of $\log_{10}(G_\infty)$ obtained in Section 4.5 plotted as a function of $\log_{10}(a)$ together with the leading-order asymptotic value of G_∞ in the limit $G_\infty \to 0$, namely $G_\infty = (15a^4/32)^{1/2}$, when $s = -1$.

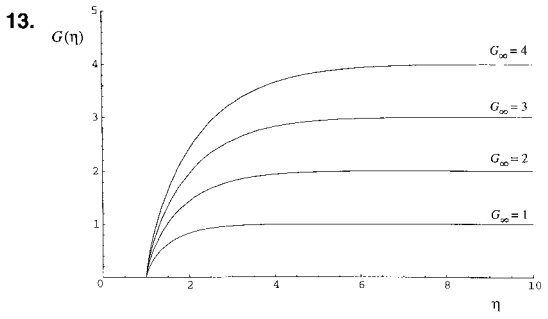

Figure 13. Numerically calculated free-surface profiles $G(\eta)$ obtained in Section 4.5 plotted as a function of η for $G_\infty = 1, 2, 3, 4$ when $s = -1$.

case $s = -1$, Equation (70) represents a unique solution for h for each value of G_∞. The solution (70) represents both a narrowing ($y_e' < 0$) dry patch with $s = -1$ in $x \leq x_0$ (which is analogous to the case $\cos\alpha < 0$ in Section 3), and a widening ($y_e' > 0$) dry patch with $s = 1$ in $x \geq x_0$ (which is analogous to the case $\cos\alpha > 0$ in Section 3). Provided that $\theta(x_0)$ is finite and non-zero for $|x_0| < \infty$ we have $J = O(x - x_0)$ as $x \to x_0$, and hence $y_e = O(|x - x_0|^{1/4})$ in this limit.

From (45) and (46) the conditions for this solution to be valid can be expressed as $\epsilon \ll 1$, $\delta \ll 1$,

$$l \ll \left(\frac{\lambda^3|T_r - T_\infty|^3}{(\rho g \sin\alpha)^2 Q\mu}\right)^{\frac{1}{3}}, \quad l \ll \left(\frac{\lambda^2(T_r - T_\infty)^2\gamma_r}{(\rho g\cos\alpha)^2 Q\mu}\right)^{\frac{1}{3}},$$
$$l \ll \left(\frac{k_{th}^2\gamma_r}{\alpha_{th}^2\lambda|T_r - T_\infty|}\right)^{\frac{1}{2}}, \quad l \ll \frac{\lambda|T_r - T_\infty|}{\tau}, \quad \frac{\lambda|T_r - T_\infty|}{\gamma_r} \ll 1. \tag{71}$$

As an example we consider again the case of a power-law substrate temperature gradient with $\theta = x^k$ for $x \geq 0$. In the general case $k \neq 1/2$ the solution (70) is

$$h = \left(\frac{2}{x^k G_\infty^2}\right)^{\frac{1}{2}} G\left(\frac{y}{y_e}\right), \quad y_e = \left|\frac{8(x^{1-2k} - x_0^{1-2k})}{3(1-2k)G_\infty^2}\right|^{\frac{1}{4}}, \tag{72}$$

and in the special case $k = 1/2$ it is

$$h = \left(\frac{4}{xG_\infty^4}\right)^{\frac{1}{4}} G\left(\frac{y}{y_e}\right), \quad y_e = \left|\frac{8\log x/x_0}{3G_\infty^2}\right|^{\frac{1}{4}}. \tag{73}$$

In particular, in the special case of a uniform temperature gradient $\theta = 1$ (that is, when $k = 0$) we find from (72) that $y_e = |8(x - x_0)/3G_\infty^2|^{1/4}$ and $h \to 2^{1/2}$ as $|y| \to \infty$, so that the film is again of uniform thickness far from the dry patch.

In the case $s = -1$ the solutions for y_e and h are qualitatively similar to those given in Section 3.5 and so examples are omitted for the sake of brevity. However in the case $s = 1$ the solution has a capillary ridge near the contact line. This latter behaviour is illustrated in

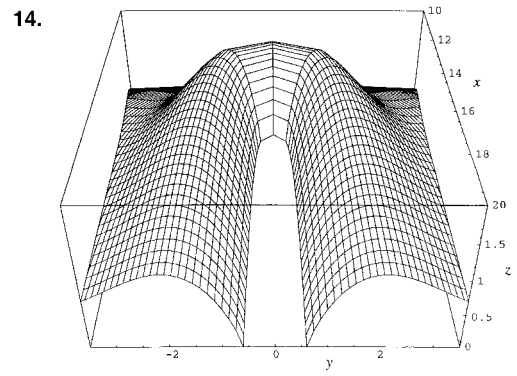

Figure 14. Numerically calculated three-dimensional plot of the solution h given by (72) in the case $\theta = x$ when $s = 1$, $\phi = 0$ and $x_0 = 10$.

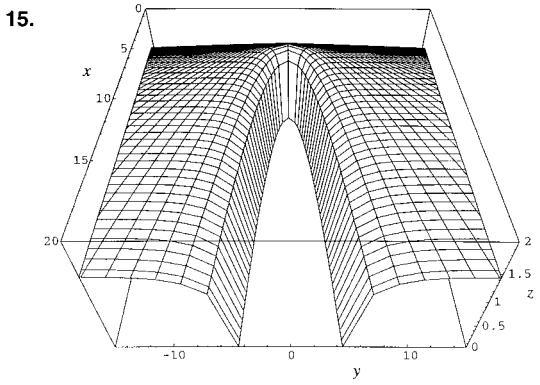

Figure 15. A gravity-driven flow with a dry patch widening or narrowing due to thermocapillarity: three-dimensional plot of the solution h given by (85) in the case $\sigma_T = -1$ when $c = 1$.

Figure 14, which shows the solution for h in the case $\theta = x$ (*i.e.*, $k = 1$) when $s = 1$, $\phi = 0$ and $x_0 = 10$.

For $x_0 > 0$ we have $y_e = O(1)$ as $x \to 0^+$ when $k < 1/2$, and $y_e = O(x^n)$ as $x \to 0^+$ when $k > 1/2$, where $n = (1-2k)/4$. On the other hand, for $x_0 = 0$ (in which case $k < 1/2$) we have $y_e = O(x^n)$ as $x \to 0^+$. Moreover for $x_0 < \infty$ we have $y_e = O(x^n)$ as $x \to \infty$ when $k < 1/2$, and for $0 < x_0 < \infty$ we have $y_e = O(1)$ as $x \to \infty$ when $k > 1/2$. On the other hand, for $x_0 = \infty$ (in which case $k > 1/2$) we have $y_e = O(x^n)$ as $x \to \infty$. In the special case $k = 1/2$ for $0 < x_0 < \infty$ we have $y_e = O(|\log x|^{1/4})$ both as $x \to 0^+$ and as $x \to \infty$.

Holland [11] gives details of the solution (70) for the two further choices of the substrate temperature gradient mentioned in Section 3.5.

5. Gravity-driven flow with a dry patch widening or narrowing due to thermocapillarity

In this section we consider gravity-driven flow down a uniformly heated or cooled substrate (so that $T_0 \equiv 1$) with a dry patch that is widening or narrowing due to thermocapillarity (*i.e.*, the case in which the fourth and fifth terms dominate (3) and the gravity term dominates (9)). Setting $\epsilon S \sin\alpha/\delta = B/\epsilon^2|\Delta C| = 1$, we find that ϵ, δ and U are given by

$$\epsilon = \left(\frac{\alpha_{\rm th}\lambda|T_{\rm r} - T_\infty|}{k_{\rm th}\rho g \sin\alpha l}\right)^{\frac{1}{2}} \ll 1, \quad \delta = \left(\frac{k_{\rm th}^3 \rho g \sin\alpha Q^2\mu^2}{\alpha_{\rm th}^3\lambda^3|T_{\rm r} - T_\infty|^3 l^3}\right)^{\frac{1}{6}} \ll 1, \quad U = \left(\frac{\rho g \sin\alpha Q^2}{\mu}\right)^{\frac{1}{3}}. \tag{74}$$

The remaining terms in (3) and (9) are negligible provided that

$$\frac{1}{C} \ll 1, \quad \tau \ll 1, \quad \frac{\delta}{\epsilon} \ll |\tan\alpha|, \tag{75}$$

which, in particular, mean that surface tension and surface shear stress must be sufficiently small, and that α is not near 0 or π (so that the substrate is not horizontal or nearly horizontal).

Similarity solutions cannot be found when $B \neq 0$, and therefore we restrict our attention to the adiabatic limit $B \to 0$. In this case the governing equations (3) and (9) reduce to

$$\sigma_T (h^3)_{yy} + 2(h^3)_x = 0 \tag{76}$$

and

$$1 = \frac{h_\infty^3}{3} \tag{77}$$

at leading order, where σ_T is given by (18).

Seeking a solution of (76) and (77) in the form (10), we have

$$(G^3)'' + 6\sigma_T \left(\frac{f' y_\mathrm{e}^2}{f} G^3 - y_\mathrm{e} y_\mathrm{e}' \eta G^2 G' \right) = 0 \tag{78}$$

and

$$1 = \frac{(bf G_\infty)^3}{3}. \tag{79}$$

In this case we find that the relevant forms for f and y_e are

$$f = 1, \quad y_\mathrm{e} = (cx)^{\frac{1}{2}}, \tag{80}$$

with the constant c to be determined; without loss of generality we have taken $x_0 = 0$ here. Note that the dry patch has a parabolic shape, and that since $f = 1$ the film is of uniform thickness far from the dry patch in this case. Then from (78) the equation for G is

$$(G^3)'' - c\sigma_T \eta (G^3)' = 0. \tag{81}$$

With the choice $b = 3^{1/3}$ the flux condition (79) yields $G_\infty = 1$. Thus solving (81) using the conditions (11) and (12), we find that

$$G = \left[\frac{\mathrm{erf}(K\eta) - \mathrm{erf}(K)}{1 - \mathrm{erf}(K)} \right]^{\frac{1}{3}} \tag{82}$$

for $c\sigma_T < 0$, where we have defined $K = (-c\sigma_T/2)^{1/2} > 0$, which satisfies

$$G = \left[\frac{2K \exp(-K^2)}{\sqrt{\pi}(1 - \mathrm{erf}(K))} \right]^{\frac{1}{3}} (\eta - 1)^{\frac{1}{3}} + O(\eta - 1)^{\frac{4}{3}} \tag{83}$$

as $\eta \to 1^+$ and

$$G \sim 1 - \frac{\eta^{-1} \exp(-K^2\eta^2)}{3\sqrt{\pi} K (1 - \mathrm{erf}(K))} \tag{84}$$

as $\eta \to \infty$. Hence the solution takes the form

$$h = \left[\frac{3 \left\{ \mathrm{erf}\left(-\frac{\sigma_T y^2}{2x} \right)^{\frac{1}{2}} - \mathrm{erf}\left(-\frac{\sigma_T y_\mathrm{e}^2}{2x} \right)^{\frac{1}{2}} \right\}}{1 - \mathrm{erf}\left(-\frac{\sigma_T y_\mathrm{e}^2}{2x} \right)^{\frac{1}{2}}} \right]^{\frac{1}{3}}, \quad y_\mathrm{e} = (cx)^{\frac{1}{2}}, \tag{85}$$

which is valid only for $\sigma_T x < 0$.

The solution (85) is unique for each value of the parameter c; this solution represents both a narrowing ($y_e' < 0$) dry patch in $x < 0$ when the substrate is heated ($\sigma_T = 1$), and a widening ($y_e' > 0$) dry patch in $x > 0$ when the substrate is cooled ($\sigma_T = -1$). The free-surface temperature $(1 + Bh)^{-1} = 1 - Bh + O(B^2)$ is a decreasing function of h. In the case when the substrate is heated ($\sigma_T = 1$) the surface tension $\gamma = 1 + \sigma_T \delta^2 Ch(1 + Bh)^{-1} = 1 + \sigma_T \delta^2 Ch + O(B)$ is an increasing function of h, and hence there is a gradient of surface tension that drives a transverse flux outwards away from $y = \pm y_e$ and towards $y = \pm\infty$, counter-intuitively causing the dry patch to narrow. In the case when the substrate is cooled ($\sigma_T = -1$) the converse holds, causing the dry patch to widen. Figure 15 shows the solution for h in the case $\sigma_T = -1$ when $c = 1$; the corresponding solution in the case $\sigma_T = 1$ is a reflection of this in the plane $x = 0$. Note that the free-surface profile in this case has a monotonically increasing shape, and that $h \to h_\infty = 3^{1/3}$ as $|y| \to \infty$.

From (74) and (75) the conditions for this solution to be valid can be expressed as $\epsilon \ll 1$, $\delta \ll 1$,

$$\left(\frac{k_{th}^6(\rho g \sin\alpha)^2 \gamma_r^3 Q\mu}{\alpha_{th}^6 \lambda^6 (T_r - T_\infty)^6}\right)^{\frac{1}{3}} \ll l, \quad \frac{\tau^3}{(\rho g \sin\alpha)^2 Q\mu} \ll 1, \quad 1 \ll \frac{\alpha_{th}^3 \lambda^3 |T_r - T_\infty|^3 |\tan\alpha|^3}{k_{th}^3 (\rho g \sin\alpha)^2 Q\mu}. \tag{86}$$

6. Shear-stress-driven flow with a dry patch widening or narrowing due to thermocapillarity

In this section we consider shear-stress-driven flow down a uniformly heated or cooled substrate (so that, as in Section 5, $T_0 \equiv 1$) with a dry patch that is widening or narrowing due to thermocapillarity (*i.e.*, the case in which the fourth and sixth terms dominate (3) and the shear-stress term dominates (9)). Setting $\tau = B/\epsilon^2|\Delta C| = 1$, we find that ϵ, δ and U are given by

$$\epsilon = \left(\frac{\alpha_{th}^2 \lambda^2 (T_r - T_\infty)^2 Q\mu}{k_{th}^2 l^2 \tau^3}\right)^{\frac{1}{4}} \ll 1, \quad \delta = \left(\frac{k_{th}^2 Q\mu\tau}{\alpha_{th}^2 \lambda^2 (T_r - T_\infty)^2 l^2}\right)^{\frac{1}{4}} \ll 1, \quad U = \left(\frac{Q\tau}{\mu}\right)^{\frac{1}{2}}. \tag{87}$$

The remaining terms in (3) and (9) are negligible provided that

$$\frac{\epsilon S \sin\alpha}{\delta} \ll 1, \quad S|\cos\alpha| \ll 1, \quad \frac{1}{C} \ll 1, \tag{88}$$

which, in particular, mean that gravity and surface tension must be sufficiently small; however, unlike in the case considered in Section 5, there is no restriction on α and so the solutions are valid for $0 \le \alpha \le \pi$. As in Section 5, we restrict our attention to the adiabatic limit $B \to 0$. In this case the governing equations (3) and (9) reduce to

$$\sigma_T (h^3)_{yy} + 3(h^2)_x = 0 \tag{89}$$

and

$$1 = \frac{h_\infty^2}{2} \tag{90}$$

at leading order, where σ_T is given by (18).

Seeking a solution of (89) and (90) in the form (10), we have

$$(G^3)'' + \frac{6\sigma_T}{b}\left(\frac{f' y_e^2}{f^2}G^2 - \frac{y_e y_e'}{f}\eta G G'\right) = 0 \tag{91}$$

and

$$1 = \frac{(bfG_\infty)^2}{2}. \tag{92}$$

In this case we find that the relevant forms for f and y_e are again given by (80) with the constant c to be determined; without loss of generality we have again taken $x_0 = 0$ here. Note that, as in Section 5, the dry patch has a parabolic shape, and the film is of uniform thickness far from the dry patch in this case. With the choice $b = 3|c|$ Equation (91) reduces to

$$(G^3)'' - s\eta G G' = 0, \tag{93}$$

where $s = \sigma_T \mathrm{sgn}(c)$, and the flux condition (92) becomes

$$1 = \frac{(3cG_\infty)^2}{2}. \tag{94}$$

As in Sections 3 and 4, the exact solution of (93) that satisfies (11) and (12) has not been found; however, again considerable analytical progress can still be made and the equation can be solved numerically.

6.1. Behaviour as $\eta \to 1^+$

The local behaviour of G as $\eta \to 1^+$ is given either by

$$G = a(\eta - 1)^{\frac{1}{3}} + \frac{s}{10}(\eta - 1) + o(\eta - 1) \tag{95}$$

for $s = \pm 1$, where $a > 0$ is an arbitrary constant, or by

$$G = \frac{s}{6}(\eta - 1) + \frac{s}{18}(\eta - 1)^2 + o(\eta - 1)^2 \tag{96}$$

for $s = 1$ only. Note that (95) (but not (96) implies that $G'(1) = \infty$ and hence the lubrication approximation fails near $\eta = 1$ in that case. There is no immediate reason for disregarding either (95) or (96); however, as we shall see shortly, there is no solution with the appropriate behaviour as $\eta \to \infty$ when $s = 1$, and so the local behaviour of G as $\eta \to 1^+$ is given by (95) with $s = -1$.

6.2. Behaviour as $\eta \to \infty$

As $\eta \to \infty$ we have $G \sim G_\infty$, and so writing $G = G_\infty + G_1$ in (93) and linearising for small G_1 gives

$$3G_\infty G_1'' - s\eta G_1' = 0. \tag{97}$$

A solution for G_1 is possible only when $s = -1$; therefore for the remainder of Section 6 we shall consider only the case $s = -1$. Equation (97) can be integrated directly to yield

$$G_1 = A\left(\frac{\pi}{6G_\infty}\right)^{\frac{1}{2}}\left[1 - \mathrm{erf}\left(\frac{\eta^2}{6G_\infty}\right)^{\frac{1}{2}}\right], \tag{98}$$

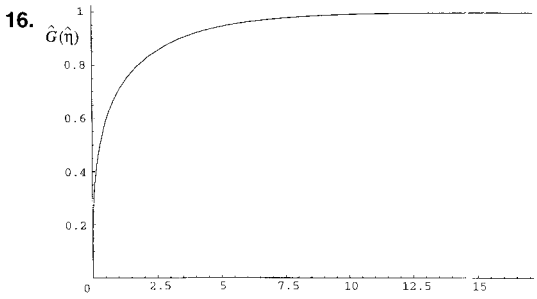

Figure 16. A shear-stress-driven flow with a dry patch widening or narrowing due to thermocapillarity: the inner solution for the free-surface profile in the limit $G_\infty \to 0$, $\hat{G}(\hat{\eta})$, given by (102) plotted as a function of $\hat{\eta}$.

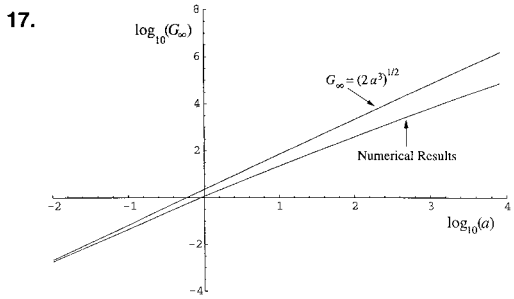

Figure 17. Numerically calculated values of $\log_{10}(G_\infty)$ obtained in Section 6.4 plotted as a function of $\log_{10}(a)$ together with the leading-order asymptotic value of G_∞ in the limit $G_\infty \to 0$, namely $G_\infty = (2a^3)^{1/2}$.

where A is an undetermined real constant. Therefore

$$G \sim G_\infty + A\eta^{-1} \exp\left(-\frac{\eta^2}{6G_\infty}\right) \tag{99}$$

as $\eta \to \infty$, and hence G approaches G_∞ monotonically in this limit.

6.3. The singular limit $G_\infty \to 0$

In the singular limit $G_\infty \to 0$ we write $G = G_\infty \widehat{G}$ so that (93) becomes

$$G_\infty(\widehat{G}^3)'' + \eta\widehat{G}\widehat{G}' = 0. \tag{100}$$

In the limit $G_\infty \to 0$ the leading-order version of Equation (100) is again $\widehat{G}' = 0$, and so the appropriate outer solution is simply $\widehat{G} = 1$. As in Sections 3.3 and 4.3, this outer solution fails near the contact line $\eta = 1$. In the inner region we introduce a rescaled coordinate defined by $\eta = 1 + G_\infty\hat{\eta}$, and hence at leading order (100) becomes

$$\widehat{G}' = \frac{1}{6}(\widehat{G}^{-2} - 1). \tag{101}$$

Solving (101), using the contact-line condition $\widehat{G} = 0$ at $\hat{\eta} = 0$, we obtain the implicit solution

$$\hat{\eta} = 6(\tanh^{-1}\widehat{G} - \widehat{G}), \tag{102}$$

which is shown in Figure 16. The uniformly valid leading-order composite solution is simply

$$G = G_\infty \widehat{G}\left(\frac{\eta - 1}{G_\infty}\right). \tag{103}$$

In particular, in the limit $\eta \to 1^+$ this solution satisfies

$$G = \left(\frac{G_\infty^2}{2}\right)^{\frac{1}{3}} (\eta - 1)^{\frac{1}{3}} - \frac{1}{10}(\eta - 1) + o(\eta - 1), \tag{104}$$

which coincides with (95) up to the order shown provided that $a = (G_\infty^2/2)^{1/3}$ and $s = -1$. Moreover, in the limit $\eta \to \infty$ we have

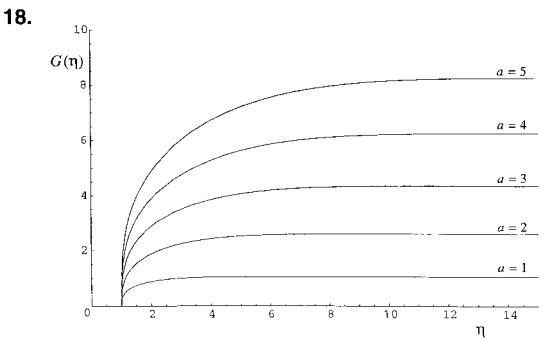

Figure 18. Numerically calculated free-surface profiles $G(\eta)$ obtained in Section 6.4 plotted as a function of η for $a = 1, 2, \ldots, 5$.

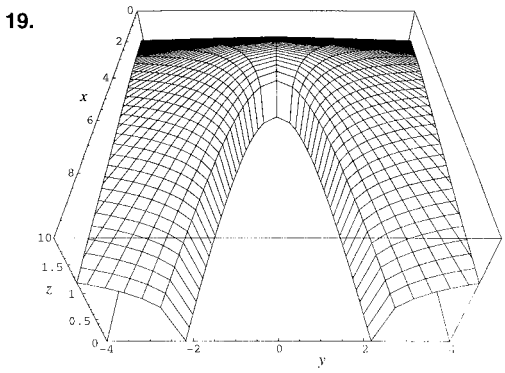

Figure 19. Numerically calculated three-dimensional plot of the solution h given by (107) in the case $\sigma_T = -1$ when $G_\infty = 1$ ($c = 2^{1/2}/3$).

$$G \sim G_\infty - 2G_\infty \exp\left(-2 + \frac{1}{3G_\infty}\right) \exp\left(-\frac{\eta}{3G_\infty}\right); \tag{105}$$

this differs somewhat from (99), but shows that G still approaches G_∞ monotonically in this limit.

6.4. Numerical solution

The system (11), (12) and (93) was solved numerically using the method described in Section 3.4. It was found that a real and positive solution for G is possible only when $s = -1$ (which is consistent with Section 6.2). The numerical calculations were started from $\eta = 1+\zeta$ for sufficiently small $\zeta \ll 1$ by using (95) to give the approximate initial conditions

$$G(1+\zeta) = a\zeta^{\frac{1}{3}} - \frac{1}{10}\zeta, \quad G'(1+\zeta) = \frac{a}{3}\zeta^{-\frac{2}{3}} - \frac{1}{10}. \tag{106}$$

Figure 17 shows the relationship between a and G_∞, and compares it with the leading-order asymptotic solution in the limit $G_\infty \to \infty$ calculated in Section 6.3, namely $G_\infty = (2a^3)^{1/2}$; clearly there is excellent agreement for sufficiently small values of G_∞. Typical free-surface profiles are shown in Figure 18 for a range of values of a. Note that all the free-surface profiles in Figure 18 have a monotonically increasing shape.

6.5. Solution for h

The solution takes the form

$$h = 3|c|G\left(\frac{y}{y_e}\right) = \left(\frac{2}{G_\infty^2}\right)^{\frac{1}{2}} G\left(\frac{y}{y_e}\right), \quad y_e = (cx)^{\frac{1}{2}} = \left(-\frac{\sqrt{2}\sigma_T x}{3G_\infty}\right)^{\frac{1}{2}}, \tag{107}$$

where G satisfies (93), which is valid only for $\sigma_T x < 0$. The solution (107) is unique for each value of G_∞ or c; this solution represents both a narrowing ($y_e' < 0$) dry patch in $x < 0$ when the substrate is heated ($\sigma_T = 1$), and a widening ($y_e' > 0$) dry patch in $x > 0$ when the substrate is cooled ($\sigma_T = -1$). This behaviour is qualitatively the same as that described

in Section 5 and has the same physical explanation. Figure 19 shows the solution for h in the case $\sigma_T = -1$ when $G_\infty = 1$ ($c = 2^{1/2}/3$); the corresponding solution in the case $\sigma_T = 1$ is a reflection of this in the plane $x = 0$. Note that the free-surface profile in this case has a monotonically increasing shape, and that $h \to h_\infty = 2^{1/2}$ as $|y| \to \infty$.

From (87) and (88) the conditions for this solution to be valid can be expressed as $\epsilon \ll 1$, $\delta \ll 1$,

$$1 \ll \frac{\tau^3}{(\rho g \sin\alpha)^2 Q\mu}, \quad \frac{k_{\rm th}^2(\rho g\cos\alpha)^2 Q\mu}{\alpha_{\rm th}^2\lambda^2(T_{\rm r}-T_\infty)^2\tau} \ll 1, \quad \frac{k_{\rm th}^2\gamma_{\rm r}\tau}{\alpha_{\rm th}^2\lambda^2(T_{\rm r}-T_\infty)^2} \ll l. \tag{108}$$

7. Conclusions

In this paper we have used the lubrication approximation to investigate slender dry patches in an infinitely wide film of viscous fluid flowing steadily on an inclined plane that is either heated or cooled relative to the surrounding atmosphere. Four non-isothermal situations in which thermocapillary effects play a significant role have been considered.

Similarity solutions describing a thermocapillary-driven flow with a dry patch that is widening or narrowing due to either gravitational or surface-tension effects on a non-uniformly heated or cooled substrate have been obtained, and we presented examples of these solutions when the substrate temperature gradient depends on the longitudinal coordinate x according to a general power law. In the case of strong gravitational effects the solution contains the free parameter $G_\infty > 0$, and for each value of this parameter there is a unique solution representing both a narrowing pendent dry patch and a widening sessile dry patch, whose transverse profile has a monotonically increasing shape. In the case of strong surface-tension effects the solution also contains the free parameter G_∞, and for each value of this parameter there is both a unique solution representing a narrowing dry patch, whose transverse profile has a monotonically increasing shape, and a one-parameter family of solutions (parameterised by ϕ) representing a widening dry patch, whose transverse profile has a capillary ridge near the contact line and decays in an oscillatory manner far from it.

We have also obtained similarity solutions describing both a gravity-driven and a constant-surface-shear-stress-driven flow with a dry patch that is widening or narrowing due to thermocapillarity on a uniformly heated or cooled substrate. The solutions in both cases contain a free parameter (c in the former case, G_∞ or c in the latter one) and for each value of this parameter there is a unique solution representing both a narrowing dry patch on a heated substrate and a widening dry patch on a cooled substrate, whose transverse profile has a monotonically increasing shape.

Note that all the present dry-patch similarity solutions (like the isothermal dry-patch similarity solutions obtained by Wilson *et al.* [6]) are valid only away from the contact line where the lubrication approximation fails because they have infinite slope, and hence to obtain the complete solution it would be necessary to formulate and solve the appropriate 'inner' Stokes-flow problem valid near the contact line subject to appropriate matching conditions with the present 'outer' similarity solutions valid far from the contact line.

As far as the authors are aware, there are no experimental results for non-isothermal dry patches with which the present analytical solutions may be compared. However, we note that experimental results for isothermal dry patches show the existence of a maximum critical volume flux for a dry patch to occur, while the present solutions (in common with the corresponding isothermal solutions of Wilson *et al.* [6]) predict either that a dry patch can occur

for all values of the flux or that there is a minimum critical flux for a dry patch to occur, *i.e.*, they are not able to predict the expected maximum critical flux without invoking an additional assumption.

Acknowledgements

The first author (DH) wishes to thank the Engineering and Physical Sciences Research Council for financial support via a studentship during the course of the present work. The second author (SKW) gratefully acknowledges the ongoing financial support of the Leverhulme Trust via a Research Fellowship.

Appendix

In this appendix we present two new local solutions near $\eta = 1$ for an isothermal gravity-driven dry patch with strong surface-tension effects that were omitted from Section 5.1 of Wilson *et al.* [6], namely

$$G = a_1(\eta - 1) + a_2(\eta - 1)^2 + \frac{1}{6}(\eta - 1)^3 + \frac{1}{32}(\eta - 1)^4 + O(\eta - 1)^5, \tag{A1}$$

where $a_1 > 0$ and a_2 are arbitrary constants, and

$$G = a_2(\eta - 1)^2 + \frac{1}{6}(\eta - 1)^3 + \frac{1}{28}(\eta - 1)^4 + O(\eta - 1)^5, \tag{A2}$$

where $a_2 > 0$ is an arbitrary constant. However, the numerical results presented in Section 5.4 of Wilson *et al.* [6] indicate that the behaviour in the limit $\eta \to 1^+$ is always given by their (5.3) and not (A1) or (A2), and therefore the rest of their paper is unaffected by the existence of these additional solutions.

References

1. D. E. Hartley and W. Murgatroyd, Criteria for the break-up of thin liquid layers flowing isothermally over solid surfaces. *Int. J. Heat Mass Transfer* 7 (1964) 1003–1015.
2. A. B. Ponter, G. A. Davies, T. K. Ross and P. G. Thornley, The influence of mass transfer on liquid film breakdown. *Int. J. Heat Mass Transfer* 10 (1967) 349–359.
3. T. Podgorski, J.-M. Flesselles and L. Limat, Dry arches within flowing films. *Phys. Fluids* 11 (1999) 845–852.
4. W. Murgatroyd, The role of shear and form forces in the stability of a dry patch in two-phase film flow. *Int. J. Heat Mass Transfer* 8 (1965) 297–301.
5. S. D. R. Wilson, The stability of a dry patch on a wetted wall. *Int. J. Heat Mass Transfer* 17 (1974) 1607–1615.
6. S. K. Wilson, B. R. Duffy and S. H. Davis, On a slender dry patch in a liquid film draining under gravity down an inclined plane. *Euro. J. Appl. Math.* 12 (2001) 233–252.
7. N. Zuber and F. W. Staub, Stability of dry patches forming in liquid films flowing over heated surfaces. *Int. J. Heat Mass Transfer* 9 (1966) 897–905.
8. G. D. McPherson, Axial stability of the dry patch formed in dryout of a two-phase annular flow. *Int. J. Heat Mass Transfer* 13 (1970) 1133–1152.
9. J. C. Chung and S. G. Bankoff, Initial breakdown of a heated liquid film in cocurrent two-component annular flow: II. Rivulet and drypatch models. *Chem. Eng. Comm.* 4 (1980) 455–470.
10. D. Holland, S. K. Wilson and B. R. Duffy, Similarity solutions for slender rivulets with thermocapillarity. Submitted to *Q. J. Mech. Appl. Math.* December 2001.
11. D. Holland, Thermocapillary effects in thin-film flows. Ph. D.thesis, University of Strathclyde, Glasgow, United Kingdom, 2002.
12. P. C. Smith, A similarity solution for slow viscous flow down an inclined plane. *J. Fluid Mech.* 58 (1973) 275–288.
13. B. R. Duffy and H. K. Moffatt, A similarity solution for viscous source flow on a vertical plane. *Euro. J. Appl. Math.* 8 (1997) 37–47.